4-1-2019

Visual Voltammogram at an Array of Closed Bipolar Electrodes in a Ladder Configuration

Janis S. Borchers
Iowa State University, jborch67@iastate.edu

Olga Riusech
Iowa State University

Eric Rasmussen
Iowa State University, ericr@iastate.edu

Robbyn K. Anand
Iowa State University, rkanand@iastate.edu

Visual Voltammogram at an Array of Closed Bipolar Electrodes in a Ladder Configuration

Abstract

In this paper, we report a method for obtaining a visual voltammogram at a linear array of closed wireless bipolar electrodes (BPEs). This advancement is significant, because the visual voltammogram captures the entire current–potential (*i*–*E*) relationship of a faradaic reaction in one image and is continuously generated over time. Therefore, we anticipate that this method will allow monitoring in redox systems that change over time. Further, the use of a linear array of BPEs eliminates the need to use a potentiostat and can be carried out with a simple DC power supply. Our experimental and numerical results demonstrate that the visual voltammogram is similar to a linear sweep voltammogram and therefore, information about the faradaic process can be extracted from the wave position, height, and shape.

Keywords

Bipolar electrochemistry, Voltammetry, Electrogenerated chemiluminescence, Visual voltammogram, Flow cell

Disciplines

Analytical Chemistry

Comments

This is a post-peer-review, pre-copyedit version of an article published in *Journal of Analysis and Testing*. The final authenticated version is available online at DOI: 10.1007/s41664-019-00098-9. Posted with permission.

[Prepared for publication as an Article in the *Journal of Analysis and Testing*]

Ms. ID: JOAT-D-19-00004

Visual voltammogram at an array of closed bipolar electrodes in a ladder configuration

Janis S. Borchers, Olga Riusech, Eric Rasmussen, Robbyn K. Anand*

Department of Chemistry, Iowa State University, 1605 Gilman Hall, 2415 Osborn Drive, Ames, Iowa 50011

Orcid identifier, Robbyn Anand: 0000-0003-2801-8280

*To whom correspondence should be addressed.

E-mail: rkanand@iastate.edu

Submitted: 5 January, 2019

Abstract

In this paper, we report a method for obtaining a visual voltammogram at a linear array of closed wireless bipolar electrodes (BPEs). This advancement is significant because the visual voltammogram captures the entire current-potential (*i*-*E*) relationship of a faradaic reaction in one image and is continuously generated over time. Therefore, we anticipate that this method will allow monitoring in redox systems that change over time. Further, the use of a linear array of bipolar electrodes (BPEs) eliminates the need to use a potentiostat and can be carried out with a simple DC power supply. Our experimental and numerical results demonstrate that the visual voltammogram is similar to a linear sweep voltammogram and therefore, information about the faradaic process can be extracted from the wave position, height, and shape.

Keywords

Bipolar electrochemistry, voltammetry, electrogenerated chemiluminescence, visual voltammogram, flow cell

1 Introduction

In this paper, we report a linear array of closed bipolar electrodes (BPEs) arranged to generate a visual voltammogram in a microfluidic flow cell (**Figure 1**). This advancement is significant because the visual voltammogram that is produced captures the entire current-potential (*i*-*E*) relationship of a faradaic process in one image and therefore, does not lose crucial thermodynamic and kinetic information. Importantly, the use of wireless electrodes obviates the need for a potentiostat and therefore, the *i*-*E* curve can be obtained with a simple DC power supply. While other methods for obtaining an *i*-*E* curve with wireless electrodes have been reported previously

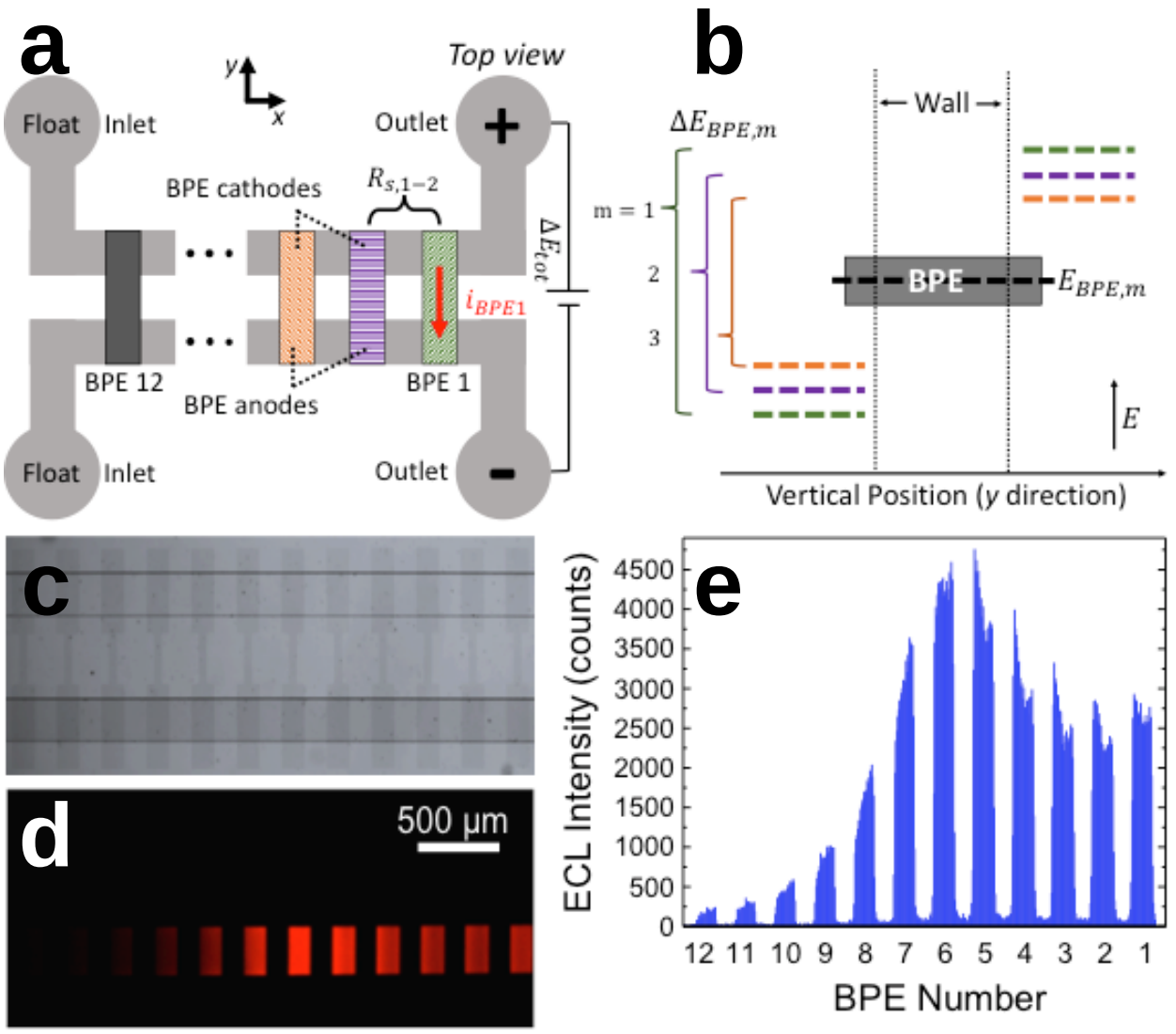

Figure 1. (a) Top view schematic illustration of the closed bipolar electrode array intersecting two parallel microfluidic channels. A voltage bias is applied between the two outlets. (b) Diagram of the solution potential in contact with the ends of the m^{th} BPE, which are fluidically isolated by the insulating wall that separates the microchannels. The difference in solution potential across each BPE ($\Delta E_{BPE,m}$) is available to drive electrically coupled faradaic reactions at its opposing ends. Due to a potential drop across the solution resistance (R_s) in the segments between BPEs, the magnitude of ΔE_{BPE} decreases with distance from the outlets. (c) Brightfield image of the array of BPEs. The top channel is the sensing channel and the bottom channel is the reporting channel. (d) Micrograph of the array of BPEs under dark room conditions. The sensing channel contains 5.0 mM $Fe(CN)_6^{3-}$ in 0.2 M phosphate buffer (pH 6.9) under a flow rate of 5.0 μL/min. The reporting channel contains ECL solution (5.0 mM $Ru(bpy)_3^{2+}$ and 25.0 mM TPrA in 0.2 M phosphate buffer) with no flow. Under a driving voltage of 4.0 V, a luminescent signal is obtained at several BPE anodes. (e) A line plot of ECL intensity versus axial location along the BPE array. The intensities were taken along the channel across the midline of the BPE anodes.

[1,2], this linear array has the following distinct advantages. First, the ends of the BPEs are in separate fluidic compartments so that the reagents employed for the coupled sensing and reporting

reactions do not mix – thereby removing limitations to the reactions that can be accessed. Second, the arrangement reported here supports flow-through analysis, which establishes rapid mass transfer – important for the determination of electron transfer kinetics – and allows for facile solution exchange. These features are relevant to widely separated applications of electrochemistry, such as in the characterization of electrocatalysts and in the sensing of eluents in chemical separations. For example, using our approach, the temporal evolution of an electrocatalytic reaction could be monitored over each of several potentials continuously. Further, BPEs have been shown to be a low cost, portable and highly sensitive method of detection for capillary electrophoresis [3,4]. While a single BPE provides an amperometric measurement at a single potential, our BPE ladder array could be configured to yield an entire voltammogram for each analyte band. Our findings show that the visual voltammogram obtained is analogous to a linear sweep voltammogram (LSV), exhibiting a peak in current under conditions of slow fluid flow and approaching a limiting current under rapid flow. The primary difference is that, while in a LSV, potentials are sampled over time, in the reported method, there is a distinct potential at each BPE in the array, thereby spatially sampling the entire *i*-*E* curve at all times. This approach therefore lends itself to observation of the temporal evolution of a faradaic process, such as may be caused by oxide growth or degradation of a catalytic material.

Electrochemical potential gradients are important to the generation and study of new materials [5-7] and to the interrogation of the mechanism of electrocatalytic reactions [8,9]. These potential gradients can be formed along an individual conductor by applying distinct potentials at opposing ends. In this way, Hillier and co-workers made use of the ohmic drop along an indium tin oxide (ITO) film to generate an electrochemical potential gradient [10]. They interrogated resultant faradaic processes along the surface with high spatial resolution by using scanning

electrochemical microscopy (SECM) [11-15]. A key feature of these studies is that SECM, in feedback mode, was able to ascertain the rate of product formation (e.g., H^+) along the potential gradient, and thereby produced a spatially arranged *i-E* curve for a single reaction.

The formation of potential gradients at BPEs has been more recently studied. A BPE is an electronic conductor with a floating potential – for example, a strip of a conductive material in an electrolyte solution. When an electric field is applied across the solution, the BPE floats to a potential intermediate to that present in the solution it contacts, and therefore, a gradient in interfacial potential difference develops along the BPE. If the total potential drop across the BPE, ΔE_{BPE}, is greater than the difference in onset potential between available oxidation and reduction reactions, then electrically coupled anodic and cathodic processes will occur at its opposing poles. Notably, the electrochemical gradient formed along a BPE has been exploited for materials synthesis [5,6], and screening of electrocatalysts [8]. However, the current at each potential (location) along this spatially arranged *i-E* curve is not readily quantified.

Instead, the total (or aggregate) current passing through a BPE (i_{BPE}) can be quantified by taking advantage of the fact that the coupled faradaic reactions must occur simultaneously and at equal and opposite rates ($i_{BPE} = i_{cathode} = -i_{anode}$). To measure this current (i_{BPE}), a reaction of interest, occurring at one end of the BPE, can be coupled to a 'reporting reaction', which generates a visible signal at the other end. These reporting reactions include electrogenerated chemiluminescence (ECL) [16,17], fluorogenic reactions [18], anodic stripping of a metal [9], electrochromic reactions [19-21], and motion [22]. This ability for BPEs to operate wirelessly allows for them to be arranged in an array format such that tens to thousands of BPEs can be operated from a single power source. Due to this characteristic, BPEs have been employed for array-based sensing [8,16,17,23], imaging [18], and electrocatalyst screening [8,9,24].

To obtain the *i-E* relationship for a faradaic process at a BPE, the potential available to drive the electrocatalytic reaction can be varied over time. For example, Chen et al. applied a time series of driving voltages to an array of BPEs, each modified with a different catalyst, to sample their *i-E* behavior [24]. Crooks and coworkers developed a highly practical and innovative approach to screen relative activity in which a catalytic material is spotted on one end of a fluorine-doped tin oxide (FTO) BPE that is patterned with a series of thin film bands of Cr at the opposing end [8,9]. When a driving voltage is applied, a catalytic reduction reaction occurs at the BPE cathode and is coupled to anodic stripping of Cr at the BPE anode. As the reactions progress, the Cr bands at the anodic tip are stripped first – before more inwardly located bands – owing to a greater electrochemical driving force there. Their removal decreases the effective length of the BPE, thereby decreasing the available potential (ΔE_{BPE}) over time. The effect is conceptually similar to a voltammetric sweep in that the electrochemical driving force is varied over time. The current can be inferred from the rate of Cr dissolution. An important distinction between this approach and LSV is that the current, at all times, is the aggregate current resulting from faradaic reactions occurring along the entire electrochemical potential gradient at the BPE. For this reason, while this method has been employed to obtain relative electrocatalytic activity, the extraction of specific rate constants is difficult.

A spatially arranged *i-E* curve can be obtained by utilizing an array of BPEs. Crooks and coworkers demonstrated that a series of BPEs can produce a visual voltammogram if each BPE is a different length, thus resulting in distinct magnitudes of ΔE_{BPE} at each [25]. In this study, a faradaic reaction of interest (a reduction) was coupled to ECL, and therefore, the intensity of the light produced reported the current at each BPE – through a quantitative and linear relationship [25]. This translation of an *i-E* curve into a plot of intensity versus location is termed ‘snapshot

voltammetry' and has the advantage of spatially sampling the entire *i-E* curve at all times without the need for a potentiostat. However, since both of the coupled reactions occur in a single compartment (an open BPE), the reactions that can be probed are limited by reagent compatibility, and further, certain reporting reactions (those that generate freely diffusing luminescent or fluorescent products) prohibit rapid fluid flow.

In the present work, we overcome these limitations by generating a spatially arranged *i-E* curve at an array of closed wireless electrodes, BPEs [19,20]. **Scheme 1a** depicts a closed BPE, for which the opposing ends of the electrode are fluidically separated by an insulating barrier (PDMS). In this case, the BPE is a thin conductive film contacting two microfluidic compartments.

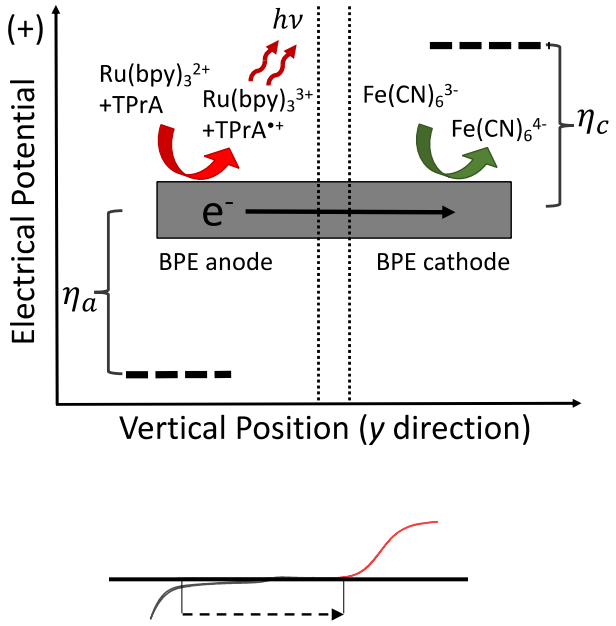

Scheme 1. Illustration of (a) the interfacial potential difference at the BPE anode and cathode and (b) the total potential across the BPE required for onset of coupled ferricyanide reduction and oxidative ECL.

The solution potential in the cathodic compartment is more negative than the potential of the BPE (E_{BPE}), thereby defining a BPE anode (depicted on the left, **Scheme 1a**). The opposite condition holds in the anodic compartment where the solution potential is more positive (BPE cathode, right side, **Scheme 1a**). The interfacial potential difference, between the solution and the electrode is an

overpotential (η_a and η_c) available to drive electrochemical oxidation and reduction at the BPE poles. In the current study, the reduction reaction occurring at each BPE cathode is reported by ECL at each BPE anode (**Scheme 1a**). The magnitude of ΔE_{BPE} required for onset of these coupled reactions is the difference between their individual onset potentials (**Scheme 1b**).

A series of distinct values of ΔE_{BPE} is achieved by arranging the BPEs in a ladder configuration (**Figure 1a,b**), such that the BPEs vary in their distance from the driving electrodes (indicated by '+' and '–' signs in outlet reservoirs, (**Figure 1a**). A key point is that this distance, along a microchannel, corresponds to an ohmic drop (iR_s) proportional to the resistance (R_s) of the intervening segment of solution, and the ionic current passing through that segment. Therefore, the potential difference across BPE 1 ($\Delta E_{BPE,1}$) is greater than that for BPE 2 ($\Delta E_{BPE,2}$) and so forth. In this study, we have configured the BPE anodes to drive ECL. Under the condition that the ECL reaction does not limit the total current (i_{BPE}), the ECL intensity reports an *i*-*E* curve (as light intensity versus BPE number, **Figure 1c-1e**) for the coupled reaction – here, the reduction of a model analyte. **Figure 1c** is a brightfield image of the array of BPEs, contacting two microchannels – the sensing channel (at top) and the reporting channel (bottom). **Figure 1d** is a micrograph of the same channel segment taken under dark room conditions. This image shows a visual voltammogram, comprising the ECL signal at each BPE anode in the reporting channel when a solution containing 5.0 mM $Fe(CN)_6^{3-}$ is flowed through the sensing channel. **Figure 1e** is a line plot of the ECL intensity (of **Figure 1d**) versus axial location along the midline of the BPE array in the reporting channel. This ECL intensity (*y*-axis) is linearly correlated to current through each BPE (i_{BPE}) while the BPE number can be correlated to potential (*E*) as described in section 3.1, below. The shape of the plot is similar to that of an LSV for $Fe(CN)_6^{3-}$ reduction – the ECL intensity increases along the BPE array with increasing η_c and reaches a maximum (peak current)

before decreasing due to mass transfer limitation. The mass transfer effect at the BPE array is explained further in section 3.5, below.

Our experimental results show that wave position is a function of driving voltage and $E^{0'}$ of the analyte. Wave height has a positive correlation to the concentration of the analyte, the number of electrons involved in a redox reaction, n, and the flow rate of the analyte solution. In addition, electrolyte concentration, acting through the solution resistance, R_s, determines the spatial distribution of the voltammogram. Finally, we show by a numerical simulation that the flow rate-dependent shape of the voltammogram, which exhibits a peak, relates to the influence of upstream diffusion layers on downstream BPEs. These findings are significant because they indicate that rich electrochemical information, similar to that obtainable by LSV at a stationary or rotating electrode subjected to a temporal potential gradient, can be obtained continuously, for all potentials simultaneously. Further, the minimal requirement of a DC power supply and the flow cell configuration hold promise for applications that demand continuous sampling or high throughput screening.

2 Experimental

2.1 Chemicals. The following chemicals were purchased and used as received: tris(2,2-bipyridine)ruthenium (II) ($Ru(bpy)_3^{2+}$), tri-*n*-propylamine (TPrA) from Sigma-Aldrich (Milwaukee, WI). ECL solution contained 5.0 mM $Ru(bpy)_3^{2+}$ and 25.0 mM TPrA in 0.2 M phosphate buffer (pH = 6.9) unless otherwise indicated. All solutions were prepared with reagent grade chemicals (Fisher Scientific, Waltham, MA) and diluted with double deionized water (18.2 MΩ•cm, Sartorius Arium Pro, Göttingen, Germany). Poly(dimethylsiloxane) (PDMS) (Sylgard 184 elastomer kit, Dow Corning Corp., Midland, MI) was used for device fabrication. Ag/AgCl

(sat. KCl) reference electrodes were purchased from Bioanalytical Systems, Inc. (West Layfette, IN).

2.2 Device fabrication and operation. Standard soft lithography [24] was used to fabricate the PDMS microfluidic flow cell. The thin film electrodes were fabricated from ITO-coated glass slides (8-12 Ω/sq) glass slides, which were purchased from Delta Technologies, Ltd., (Loveland, CO). The ITO electrodes were patterned using a positive photoresist (AZP4620, MicroChemicals GmbH, Ulm, Germany), developed with AZ 400K developer and then wet etched with aqua regia (4:1 ratio, hydrochloric acid, nitric acid) and rinsed with DI water. The photoresist was then stripped with acetone and the slide dried with a stream of N_2.

Channel molds were patterned using negative photoresist (SU-8 2015, Microchem Corp., Westborough, MD) on a Si substrate. Subsequently, PDMS precursor was poured onto the SU-8 mold and cured at 70° C for 3 h. The alignment of PDMS microchannels with BPE arrays was carried out as follows. First, the slides with the electrode pattern and PDMS channels were exposed to an air plasma (Plasma cleaner, Harrick Scientific, Ithaca, NY) for 90 s to activate the surfaces for permanent bonding. Second, a few drops of ethanol were applied on the slide to delay bonding and facilitate the alignment. Third, the aligned device was baked at 70° C for 3 h to completely drive off the ethanol and to encourage bonding.

The two microchannels of the device were 1.74 cm long, 250 μm wide, and 50 μm tall. The BPEs were each 1000 μm wide (of which 250 μm was exposed to each microchannel), 150 μm long, and spaced 150 μm from the next BPE, with the BPE nearest the driving electrodes (BPE 1) aligned 3.7 mm from the outlet reservoirs. A biopsy punch was used to create 1.0 mm-diameter inlets and 4.0 mm-diameter outlet reservoirs. Ag/AgCl driving electrodes were inserted into the

outlet reservoirs. The electric field was generated by applying a voltage bias (ΔE_{tot}) to the driving electrodes using a BK Precision 1687B power supply (Melrose, MA).

A separate device, which was employed for cyclic voltammetric measurements at a single microband electrode was comprised of one microchannel that was 1.0 cm long, 250 μm wide, and 50 μm tall with 1.0 mm and 4.0 mm inlet and outlet reservoirs, respectively. This channel overlaid a single ITO microband (250 μm wide and 150 μm long) positioned 50.0 μm from the outlet reservoir. Contact to the microband was made by copper tape, and a Pt wire auxiliary electrode and Ag/AgCl reference electrode were inserted into the outlet. Cyclic voltammetry (CV) at this microband was carried out using a Pine Research WaveDriver 40 Bipotentiostat (Durham, NC).

2.3 Microscope Images of Luminscence. A microscope (Nikon AZ100, Nikon Co., Tokyo, Japan) and a sCMOS camera (Andor Zyla 4.2, Oxford Instruments, Abingdon, Oxfordshire, England) were used to obtain luminescence micrographs under dark room conditions with a 2.0 s exposure time. Nikon Imaging Software was used to process the micrographs. To determine the average ECL intensity at each BPE, an intensity line profile was taken across the midline of the BPE (along the channel axis), then these values were background subtracted and finally averaged.

2.4 Electrochemical measurements at the BPE array. A typical experiment was performed with flow in the sensing channel at a constant rate of 5.0 μL/min, unless otherwise indicated, and still (no flow) conditions in the reporting channel. Flow was induced using a Pico Plus Elite syringe pump (Harvard Apparatus, Holliston, MA). The ECL solution, in the reporting channel, was refreshed after each change in experimental conditions, for 30 s at a flow rate of 25.0 μL/min. The flow was then stopped, and after 30 s, a voltage was applied between driving electrodes located in the two outlet reservoirs. Finally, 30 s after initiating the driving voltage, an image was obtained.

It was determined that these wait times led to the most stable ECL emission. The process was then repeated for the next experimental condition.

2.5 Modeling of fluid dynamics. The mass transfer limited current was modeled using COMSOL Multiphysics 5.4 (COMSOL, Inc., Burlington, MA). Simulation parameters assumed water was flowing through the device under three distinct flow rates (5.0, 50, and 150 μL/min) at a series of four microband electrodes, in a 3-dimensional device geometry (width, height, electrode length and spacing) matched to our BPE ladder array at room temperature. Laminar flow and transport in dilute species were considered in the physics of the model with zero velocity (no-slip condition) and zero flux at the walls.

3 Results and Discussion

3.1 Voltammetric response of the BPE array. The application of a driving voltage, ΔE_{tot}, across an ionically conductive solution in contact with a BPE, leads to an interfacial potential difference between the BPE, an equipotential object, and the solution it contacts. ΔE_{BPE} is the total potential difference experienced by the BPE and is the sum of the anodic and cathodic overpotentials (η_a and η_c) available to drive electrically coupled faradaic reactions at its opposing ends (**Scheme 1a**). Because these reactions are stoichiometrically linked by electrons, the current obtained from a redox reaction at the BPE cathode can be quantitatively reported by a light-generating reaction (ECL) at the BPE anode. The voltammogram of **Scheme 1b** depicts the magnitude of ΔE_{BPE} required for the onset of two coupled reactions – the reduction of ferricyanide and oxidative ECL.

When an array of such BPEs is arranged in a ladder configuration between two microchannels, ΔE_{BPE} experienced by each sequential BPE decreases with increased distance from the driving electrodes (positioned in the channel outlets, **Figure 1a,b**). This decrease in the

magnitude of ΔE_{BPE} from one BPE to the next results from an ohmic potential drop across the intervening solution segments (in both microchannels), and is proportional to the ionic current passing through those segments. The potential drop can be estimated by using the following restatement of Ohm's Law.

$$\Delta E_{BPE,1} - \Delta E_{BPE,2} = i_{BPE,2}(2R_{s,1-2}) \quad \text{eq 1}$$

$$R_{s,1-2} = \frac{l}{\kappa A} \quad \text{eq 2}$$

Where $\Delta E_{BPE,1}$ and $\Delta E_{BPE,2}$ are the total potential difference available to drive faradaic reactions at BPE 1 and BPE 2, respectively; $i_{BPE,2}$ is the current passing through BPE 2. Eq. 2 can be used to calculate the solution resistance, $R_{s,1-2}$, in the segment between the BPEs, where l and A are the length and cross-sectional area of the channel, and κ is the solution conductivity. Eqs 1 and 2 are formulated such that the included variables are assumed to be equivalent and constant in the two microchannels, which is the case for instance, if the same electrolyte (identical ionic strength) is used in both. For the 0.2 M phosphate buffer employed here, $R_{s,1-2}$ = 8.36 kΩ, which leads to a decrease in ΔE_{BPE} of 33.4 to 167 mV for i_{BPE} of 2.00 to 10.0 μA.

A key point is that the onset of the ECL reaction with potential is steep, and therefore, this series of ΔE_{BPE} values approximates a series of voltammetric potentials at the BPE cathodes versus an essentially constant potential at this ECL 'edge' (at the BPE anodes). This feature is important because, under the condition that the cathodic reaction limits the current at each BPE, a plot of the ECL intensity at each BPE along the array will approximate an i-E curve. In this case, BPE number is a proxy for potential (E) and ECL intensity represents the current at each BPE, $i_{BPE,m}$ (see **Figure S2**, SI). An important caveat to this analogy to a voltammogram is that the potential dropped between BPEs, due to its proportionality to $i_{BPE,m}$, grows smaller along the array. This phenomenon leads to distribution of low-current responses over a larger number of BPEs.

Given this analogy, we anticipated a voltammetric wave (in ECL intensity) with position (BPE number) correlated to the formal potential ($E^{0\prime}$) for the redox species at the BPE cathodes and height (ECL intensity) directly proportional to its bulk concentration. We further hypothesized that $\Delta E_{BPE,1}$ would be equal to ΔE_{tot} less the ohmic potential drop between the outlet reservoirs and BPE 1.

3.2 Characterization of the dependence of wave location on driving voltage. We first measured the ECL response at the BPE anodes that was obtained in the presence of two model analytes – ferricyanide ($Fe(CN)_6^{3-}$) and benzoquinone (BQ) – under a series of driving voltages. **Figure 2a** is a plot of the average ECL intensity at each BPE (BPE numbers 1-12) in the presence of 5.0 mM $Fe(CN)_6^{3-}$ in 0.2 M phosphate buffer at three distinct values of ΔE_{tot}. To obtain each voltammogram, first, the reporting channel (bottom channel, **Figure 1a**) was filled with ECL solution and then the flow stopped. Second, $Fe(CN)_6^{3-}$ solution was flowed into the sensing channel (top channel, **Figure 1a**) at a constant rate of 5.0 μL/min. Finally, ΔE_{tot} was applied at the driving electrodes, and after 30 s the ECL response at the BPE anodes was recorded.

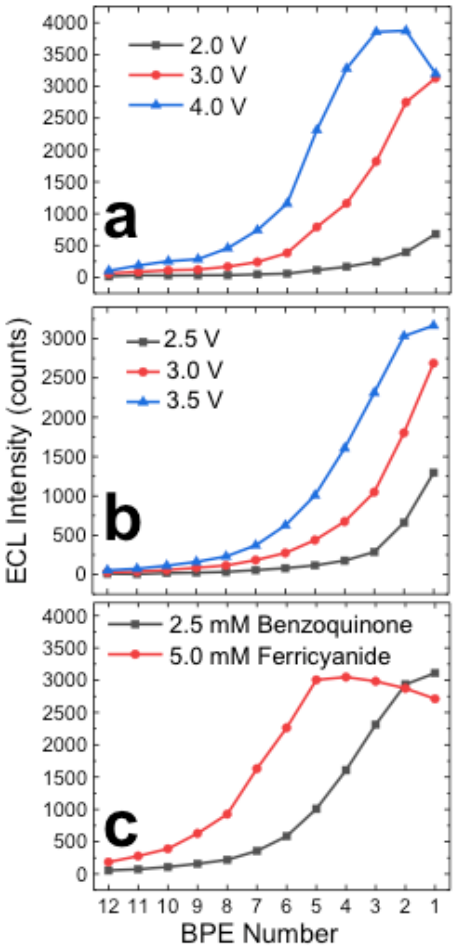

Figure 2. (a) Plot of the average ECL intensity along the axial midline of each BPE in the presence of 5.0 mM $Fe(CN)_6^{3-}$ in 0.2 M phosphate buffer at three distinct voltages, ΔE_{tot} = 2.0 V (black squares), 3.0 V (red circles), and 4.0 V (blue triangles). (b) Plot of average ECL intensity at each BPE in the presence of 2.5 mM BQ in 0.2 M phosphate buffer at ΔE_{tot} = 2.5 V (black squares), 3.0 V (red circles), and 3.5 V (blue triangles). (c) Overlay of the $Fe(CN)_6^{3-}$ and BQ responses at ΔE_{tot} = 3.5 V.

The result at ΔE_{tot} = 4.0 V (triangles) approximates the shape of an LSV, which can be explained as follows. As the $Fe(CN)_6^{3-}$ solution enters the channel, it encounters increasingly negative potentials (versus ECL) at the cathodes, from left (BPE 12) to right (BPE 1), and the rate of $Fe(CN)_6^{3-}$ reduction is concomitantly increased. An important point is that a peak in ECL intensity (current) is observed at BPEs 2 and 3, followed by a decrease at BPE 1. This feature indicates that the current for $Fe(CN)_6^{3-}$ reduction reaches a mass transfer limit at 4.0 V. The decrease in current is caused by depletion of $Fe(CN)_6^{3-}$ from the flow laminae nearest the

electrodes and is analogous to the growth of the diffusion layer in traditional voltammetry. For a subset of applications, such as sensing, the presence of a peak can provide a useful handle for data interpretation, serving a purpose similar to peak location and peak current in LSV.

Comparison of the result at ΔE_{tot} = 4.0 V with those obtained at 3.0 V and 2.0 V shows that as the driving voltage decreases, the voltammogram is shifted to earlier BPEs (i.e., from left to right, **Figure 2a**). This shift occurs because at lower ΔE_{tot}, $\Delta E_{BPE,1}$ is also decreased, and as a result, all BPE cathodes experience a less negative voltage (versus ECL). This outcome is similar to that obtained in LSV if the voltage scan is terminated at a lower (less negative) overpotential. These results verify that the BPE ladder device can be employed to obtain an i-E curve and demonstrate the relationship between $\Delta E_{BPE,1}$ and ΔE_{tot}. Note that ΔE_{tot} of 2.0 V (**Figure 2a**), at which a slight ECL signal is observed, corresponds to $\Delta E_{BPE,1}$ of approximately 1.6 V, as estimated from the R_s of the segment extending from the outlet to BPE 1. This value is slightly greater than the difference in onset potentials (~1.35 V) for the reduction of $Fe(CN)_6^{3-}$ and the ECL reaction.

3.3 Characterization of the dependence of wave location on the analyte identity. Next, to verify that the wave location is correlated with the identity of the analyte, we measured the ECL intensity obtained in response to a solution of BQ, under the same set of conditions. Because BQ reduction to hydroquinone (HQ) proceeds via the transfer of 2 electrons (as opposed to 1 electron in the case of $Fe(CN)_6^{3-}$), we used a solution of 2.5 mM BQ in 0.2 M phosphate buffer with the expectation that the peak ECL intensities (peak currents) would be similar to those obtained for 5.0 mM $Fe(CN)_6^{3-}$.

The results of BQ reduction (at ΔE_{tot} = 2.5, 3.0, and 3.5 V) are shown in **Figure 2b**. These results demonstrate once again that as ΔE_{tot} increases, the ECL intensity increases and shifts

further into the channel (to higher BPE numbers). A mass transfer (mt) limited response is not observed until the highest voltage (ΔE_{tot} = 3.5 V). **Figure 2c** is an overlay of the ferricyanide and BQ responses at ΔE_{tot} = 3.5 V. As expected, the ECL intensity is comparatively equal for the two solutions (within 2%). Further, the wave position for ferricyanide is at less negative potentials (mt

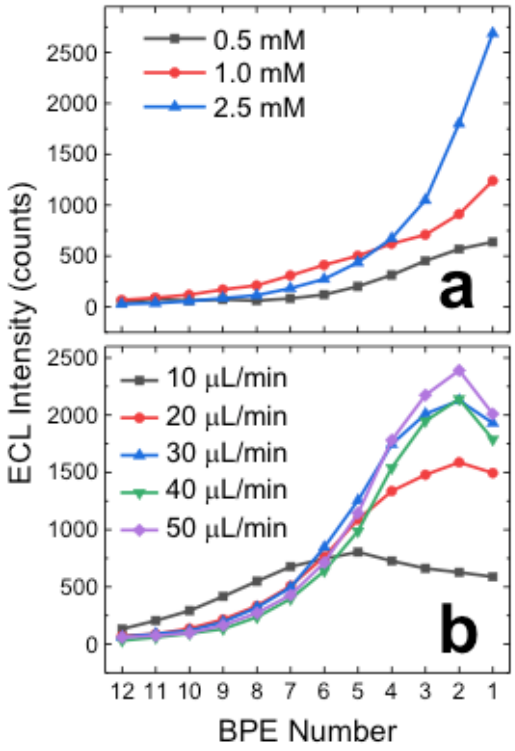

Figure 3. (a) Plot of the average ECL intensity (taken axially along the midline) of each BPE at three concentrations of BQ (0.5 mM, black squares; 1.0 mM, red circles; 2.5 mM, blue triangles) in 0.2 M phosphate buffer, in the sensing channel and at ΔE_{tot} = 3.0 V. (b) Average ECL intensity along the midline of each BPE of 2.0 mM ferricyanide in 0.2 M phosphate buffer in the sensing channel at five distinct flow rates (10, 20, 30, 40, and 50 µL/min) at ΔE_{tot} = 3.5 V.

limit at BPE 5) than that for BQ (mt limit, BPE 2).

3.4 Characterization of the dependence of wave height on analyte concentration and flow rate. To understand the dependence of the wave height on concentration of the analyte, BQ reduction at the BPE cathodes was investigated at three distinct concentrations (0.5, 1.0, and 2.5 mM), in the same device and at a constant ΔE_{tot} of 3.0 V and flow rate of 5.0 µL/min. **Figure 3a** shows the impact of the concentration of the analyte on ECL intensity. For example, at BPE 1, the

average ECL intensity increases 2-fold and 2.2-fold in the transitions from 0.5 to 1.0 mM and then to 2.5 mM. This near direct proportionality does not hold at higher BPE numbers because higher current at early BPEs (e.g., at 2.5 mM BQ) translates into a more precipitous drop-off in ΔE_{BPE}. In other words, BPE 4 thru BPE 12 experience a lower driving force for faradaic reactions in the 2.5 mM versus the 1.0 mM BQ case. Given equal ΔE_{tot}, a direct correlation between concentration and current can be predicted. Unwin and coworkers developed an equation that describes the mt-limited current anticipated at a thin-film microband electrode positioned along the floor of a microfluidic channel under conditions of fluid flow [27].

$$i_{\mathrm{lim}} = 1.165 n F c_b D^{2/3} \left(\frac{V_f}{2 h w_{ch}}\right)^{1/3} h^{-1/3} w {x_e}^{2/3} \qquad \text{eq} \quad 3$$

Here, n is the number of electrons involved in the faradaic reaction, F is Faraday's constant, c_b is the bulk concentration of a redox active species, D is the diffusion coefficient, V_f is volume flow rate, h is the half channel height, w_{ch} and w are the width of the channel and electrode, respectively, and x_e is the electrode length along the channel axis.

Equation 3 further predicts the dependence of wave height on flow rate in the analyte channel. The impact of flow rate was investigated for a solution of $Fe(CN)_6^{3-}$ (2.0 mM) in 0.2 M phosphate buffer at ΔE_{tot} = 3.5 V. **Figure 3b** is a plot of the ECL intensity obtained at the BPE array for this solution over a range of flow rates (10, 20, 30, 40, and 50 μL/min). Over the range tested, a linear dependence of current on flow rate to the one third power was observed (**Figure S1**, Supporting Information (SI)), which is in agreement with eq. 3. This result is important because it indicates that current at the BPE cathodes is limited by mass transfer and is not limited by other factors, such as the rate of the ECL reaction.

3.5 Numerical simulation of the impact of concentration depletion on the BPE array. To better understand the observed depletion effect and its dependence on flow rate, we simulated mt-

limited current under three distinct flow rates at a series of four microband electrodes, in a 3-dimensional device geometry (width, height, electrode length and spacing) matched to our BPE ladder array. **Figures 4a** and **4b** are surface plots of analyte concentration (plotted as the ratio of local concentration to that at the inlet) along the channel segment containing the first two BPEs and obtained at flow rates of 5.0 and 50 μL/min, respectively. In both cases, a region depleted of analyte develops above each electrode and reduces the flux of analyte to downstream electrodes.

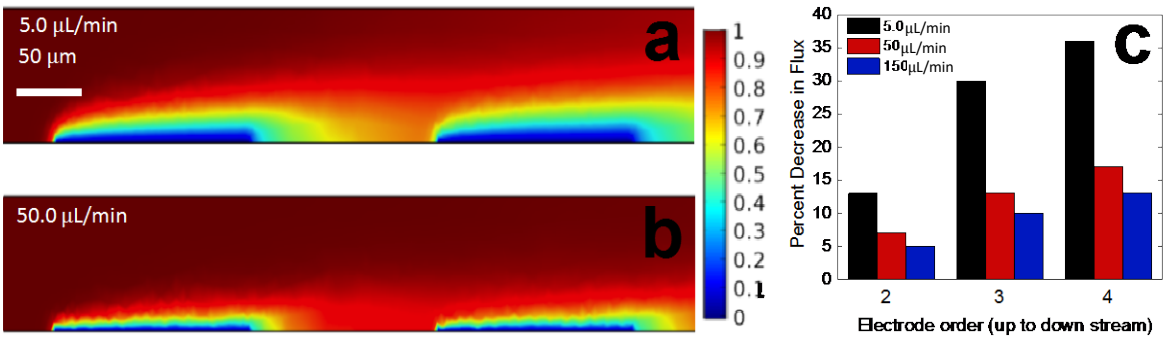

Figure 4. (a) Results of the numerical simulation at (a) 5.0 and (b) 50 μL/min flow (left to right) showing the concentration of a redox active species (relative to the concentration at the inlet) in the segment of the microchannel containing two BPEs. (c) Plot of the percent decrease in flux from the upstream electrode to each subsequent electrode at flow rates of 5.0, 50, and 150 μL/min. Average of simulated flux in the *z*-direction was taken across the entire surface of each electrode.

Figure 4c is a plot of the percent decrease in flux relative to the first (furthest upstream) electrode at each subsequent electrode. At the lower flow rate (5.0 μL/min) the difference in flux between the first (upstream) and second (downstream) electrodes is 13%, whereas at 50 μL/min, the difference is much smaller, at 7%. These numerical results confirm that the shape of the voltammogram is influenced by upstream diffusion layers on downstream BPEs. We anticipate that the shape of the voltammogram at high overpotentials (mt-limited currents) can be readily predicted. As part of our ongoing work, we are developing a more detailed model to predict the shape of the entire *i-E* curve at the BPE ladder.

3.6 Characterization of the dependence of wave distribution on electrolyte conductivity. Finally, we investigated the impact of the conductivity of the electrolyte (κ) on the spatial

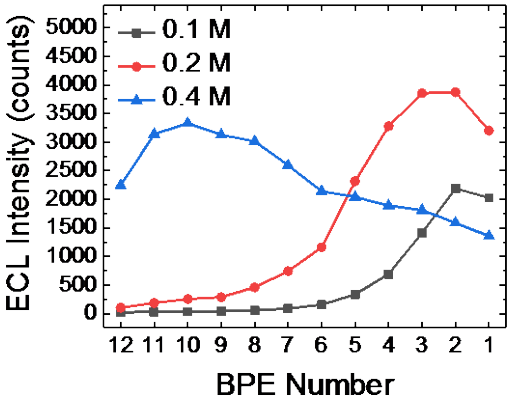

Figure 5. Plot of the average ECL intensity along the midline each BPE when the sensing channel was filled with 5.0 mM $Fe(CN)_6^{3-}$ in three distinct concentrations of phosphate buffer, 0.1 M (black squares), 0.2 M (red circles), and 0.4 M (blue triangles). Flow rate, 5.0 µL/min. $\Delta E_{tot} = 4.0$ V.

distribution of the voltammogram via the solution resistance, R_s. **Figure 5** shows the ECL response obtained at the BPE anodes with an analyte solution of 5.0 mM ferricyanide. These voltammograms were obtained using three distinct concentrations of phosphate buffer – 0.1, 0.2, and 0.4 M with conductivities of 15.9, 28.7, and 50.7 mS/cm, respectively. It should be noted, when the concentration of the phosphate buffer was changed in the sensing channel, the phosphate buffer concentration in the reporting channel was also changed to match the electrolyte concentration in the sensing channel. In all cases, ΔE_{tot} = 4.0 V and the flow rate was 5.0 µL/min. The highest electrolyte concentration (0.4 M phosphate buffer) decreased the potential increments between BPEs (as predicted by eqs 1 and 2), thereby spreading out the voltammogram. As a result, the peak ECL intensity is shifted upstream (to BPE 10) due to decreased ohmic potential drop between the driving electrodes and the BPE array. The result at 0.1 M phosphate buffer shows the opposite response and is shifted downstream due to significant resistive losses along the channel. These results indicate that the BPE ladder method is best suited for voltammetric measurements in solutions that possess uniform conductivity.

4 Conclusions

In conclusion, the ladder configuration of BPEs reported here allows a visual i-E curve to be generated and is therefore able to capture thermodynamic and kinetic information about the reaction proceeding in the sensing channel. Important features of this voltammetric technique include that (i) the i-E curve is conceptually similar to an LSV, which aids in interpretation, (ii) is continuously generated over time, thereby making this technique attractive for monitoring redox systems or sample solutions that change over time such as in electrophoretic separations, and (iii) can be accomplished with a simple power supply, or even two AA batteries (1.5 V each). This last feature is especially relevant to remote or resource-limited sensing applications. In such applications, a further advantage is that the device can be scaled such that the voltammogram is naked-eye visible, and the user can readily count the illuminated BPEs to evaluate the voltammogram.

In this preliminary characterization of the system, $Fe(CN)_6^{3-}$ and BQ were used as model analytes, and our results demonstrate that (i) wave height is directly proportional to analyte concentration and the number of electrons involved in the redox reaction and to the flow rate to the one third power as predicted by existing theoretical treatments of microband electrodes in microchannels; (ii) wave position is a function of the driving voltage and formal reduction potential of the analyte; and (iii) the spatial distribution of the voltammogram is sensitive to the electrolyte concentration. These findings are important because they indicate that key features of an i-E curve are captured by this method.

Our future work will include extension of this method to the interrogation of systems with mixed redox species and to real-time monitoring of reactions or separations processes. Current limitations of the technique must also be evaluated and addressed, such as the reliance on an ECL

reagent solution and external Ag/AgCl reference electrodes, which both could instead be integrated onto the device.

Acknowledgments

The authors thank the Society of Analytical Chemists of Pittsburgh for a Starter Grant. JSB acknowledges partial support from the Iowa State University Center for Catalysis. The authors also gratefully thank Min Li, Kira Rahn, and Beatrise Berzina for both technical support and assistance in preparing the manuscript for publication.

References

(1) Cox JT, Guerrette JP, Zhang B. Steady-State Voltammetry of a Microelectrode in a Closed Bipolar Cell. *Anal. Chem.* 2012;84:8797–804.

(2) Chang BY, Mavré F, Chow KF, Crooks JA, Crooks RM. Snapshot Voltammetry Using a Triangular Bipolar. *Anal. Chem.* 2010;82:5317–22.

(3) Klett, O.; Nyholm, L. Separation High Voltage Field Driven On-Chip Amperometric Detection in Capillary Electrophoresis. *Anal. Chem.* **2003**, *75* (6), 1245–1250.

(4) Ordeig, O.; Godino, N.; del Campo, J.; Muñoz, F. X.; Nikolajeff, F.; Nyholm, L. On-Chip Electric Field Driven Electrochemical Detection Using a Poly(Dimethylsiloxane) Microchannel with Gold Microband Electrodes. *Anal. Chem.* **2008**, *80* (10), 3622–3632.

(5) Fosdick SE, Knust KN, Scida K, Crooks RM. Bipolar Electrochemistry. *Angew. Chemie Int. Ed.* 2013;52:10438–56.

(6) Loget G, Zigah D, Bouffier L, Sojic N, Kuhn A. Bipolar Electrochemistry: From Materials Science to Motion and Beyond. *Acc. Chem. Res.* 2013;46:2513-23.

(7) Mavré F, Anand RK, Laws DR, Chow KF, Chang BY; Crooks JA, Crooks RM. Bipolar Electrodes: A Useful Tool for Concentration, Separation, and Detection of Analytes in Microelectrochemical Systems. *Anal. Chem.* 2010;82:8766–74.

(8) Fosdick SE, Crooks RM. Bipolar Electrodes for Rapid Screening of Electrocatalysts. *J. Am. Chem. Soc.* 2012;134:863–6.

(9) Fosdick SE, Berglund SP, Mullins CB, Crooks RM. Parallel Screening of Electrocatalyst Candidates Using Bipolar Electrochemistry. *Anal. Chem.* 2013;85:2493–9.

(10) Singh BK, Hillier AC. Surface Plasmon Resonance Imaging of Biomolecular Interactions on a Grating-Based Sensor Array. *Anal. Chem.* 2006;78:2009–18.

(11) Jayaraman S, Hillier AC. Construction and Reactivity Mapping of a Platinum Catalyst Gradient Using the Scanning Electrochemical Microscope. *Langmuir* 2001;17:7857–64.

(12) Jambunathan K, Jayaraman S, Hillier AC. A Multielectrode Electrochemical and Scanning Differential Electrochemical Mass Spectrometry Study of Methanol Oxidation on Electrodeposited PtxRuy. *Langmuir* 2004;20:1856–63.

(13) Mougin K, Ham AS, Lawrence MB, Fernandez EJ, Hillier AC. Construction of a Tethered Poly(Ethylene Glycol) Surface Gradient For Studies of Cell Adhesion Kinetics. *Langmuir* 2005;21:4809–12.

(14) Singh BK, Hillier AC. Surface Plasmon Resonance Imaging of Biomolecular Interactions on a Grating-Based Sensor Array. *Anal. Chem.* 2006;78:2009–18.

(15) Singh BK, Hillier AC. Surface Plasmon Resonance Enhanced Transmission of Light through Gold-Coated Diffraction Gratings. *Anal. Chem.* 2008;80:3803–10.

(16) Chow KF, Mavré F, Crooks RM. Wireless Electrochemical DNA Microarray Sensor. *J. Am. Chem. Soc.* 2008;130:7544–45.

(17) Chow KF, Mavré F, Crooks JA, Chang BY, Crooks RM. A Large-Scale, Wireless Electrochemical Bipolar Electrode Microarray. *J. Am. Chem. Soc.* 2009;131:8364–5.

(18) Guerrette JP, Percival SJ, Zhang B. Fluorescence Coupling for Direct Imaging of Electrocatalytic Heterogeneity. *J. Am. Chem. Soc.* 2013;135:855–61.

(19) Xu W, Fu K, Ma C, Bohn PW. Closed Bipolar Electrode-Enabled Dual-Cell Electrochromic Detectors for Chemical Sensing. *Analyst* 2016;141:6018–24.

(20) Xu W, Fu K, Bohn PW. Electrochromic Sensor for Multiplex Detection of Metabolites Enabled by Closed Bipolar Electrode Coupling. *ACS Sensors* 2017;2:1020–6.

(21) Zhang X, Shang C, Gu W, Xia Y, Li J, Wang E. A Renewable Display Platform Based on the Bipolar Electrochromic Electrode. *ChemElectroChem*. 2016;3:383–6.

(22) Gupta B, Goudeau B, Kuhn A. Wireless Electrochemical Actuation of Conducting Polymers. *Angew. Chem. Int. Ed. Engl.* 2017;56:14183-6.

(23) Zhang X, Zhai Q, Xing H, Li J, Wang E. Bipolar Electrodes with 100% Current Efficiency for Sensors. *ACS Sens.* 2017;2:320-6.

(24) Lin X, Zheng L, Gao G, Chi Y, Chen G. Electrochemiluminescence Imaging-Based High-Throughput Screening Platform for Electrocatalysts Used in Fuel Cells. *Anal. Chem.* 2012;84:7700–7.

(25) Mavré F, Chow KF, Sheridan E, Chang BY, Crooks JA, Crooks RM. A Theoretical and Experimental Framework for Understanding Electrogenerated Chemiluminescence (ECL) Emission at Bipolar Electrodes. *Anal. Chem.* 2009;81:6218–25.

(26) McDonald JC, Whitesides GM. Poly(Dimethylsiloxane) as a Material for Fabricating Microfluidic Devices. *Acc. Chem. Res.* 2002;35:491–9.

(27) Bitziou E, Snowden ME, Joseph MB, Leigh SJ, Covington JA, MacPherson JV, Unwin

PR. Dual Electrode Micro-Channel Flow Cell for Redox Titrations: Kinetics and Analysis of Homogeneous Ascorbic Acid Oxidation. *J. Electroanal. Chem.* 2013;692:72–9.